Supporting information

A new dynamic framework with direct *in situ* visualisation of breathing under CO_2 gas pressure

Phumile Sikiti, Charl X. Bezuidenhout, Dewald P. van Heerden, and Leonard J. Barbour*

Department of the chemistry and Polymer Science, University of Stellenbosch, Stellenbosch 7600, South Africa

1. Synthesis and characterisation

Materials

All chemicals and solvents were purchased from Aldrich and used without further purification. The ligand 4-bis(pyridin-4-ylmethyl)piperazine was prepared according to a literature procedure.[1]

Preparation of COB1-DMF

{[Co_2(OBA)$_2$(BPMP)]·2.5(DMF)$_n$ (COB1-DMF): $CO_2(NO_3)_2 6H_2O$ (1 mmol), 4,4'-oxybis(benzoic acid) (OBA, 1 mmol) and (4-bis(pyridin-4-ylmethyl)piperazine (BPMP, 1 mmol) were mixed in 2 ml methanol (MeOH) and dimethylformamide (DMF) and placed in a pre-heated oven at 80 °C. Blue block-shaped crystals of solvated (**COB1-DMF**) were obtained after 48 h.

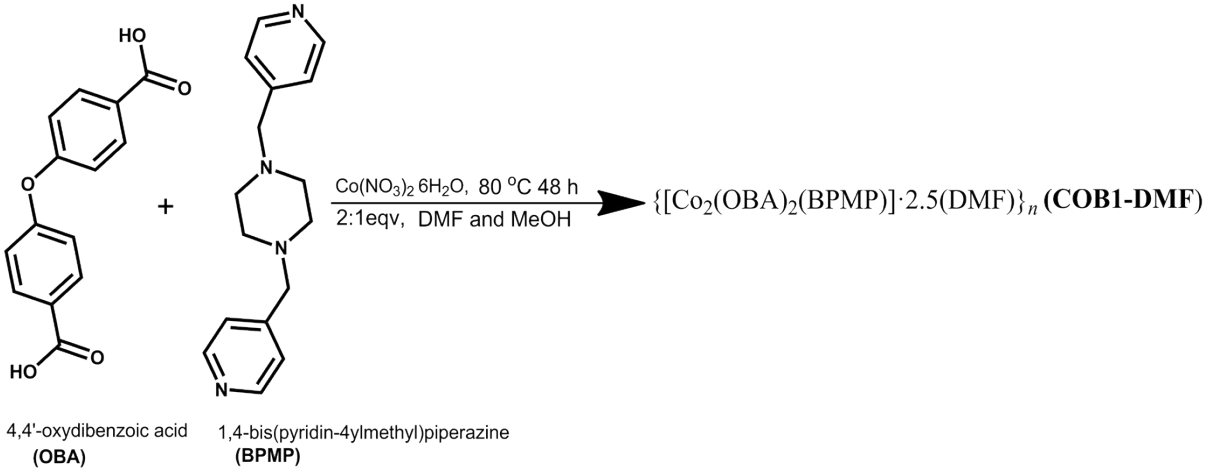

Scheme S1. Synthesis of **COB1-DMF**.

2. Methods

Thermogravimetric analysis (TGA)

Thermogravimetric analysis was carried out using a TA Instruments Q500 analyser. The sample was loaded onto an aluminium pan and heated at 10 °C/min from room temperature to 600 °C.

Activation method of COB1-DMF

Pure bulk material of **COB1-DMF** was activated at 120 °C under dynamic vacuum (3.1×10^{-2} mbar) for 12 hours to yield the fully desolvated form **COB1-act**. TGA shows that **COB1-act** is desolvated and PXRD analysis shows that it is still crystalline. Direct activation does not yield single crystals suitable for SCD analysis. Single crystals of suitable quality were obtained by activation via solvent exchange with diethyl ether for 2 days, followed by activation in a Schlenck tube at ca 195 K (slurry of dry ice and acetone) under a dynamic vacuum of 3.1×10^{-2} mbar for 48 hours. The desolvated form absorbs moisture and needed to be pre-activated under dynamic vacuum at room temperature for 2 hours before any further experiments were carried out.

Powder X-ray Diffraction (PXRD)

Experiments were carried out on a PANalytical X'Pert PRO instrument with Bragg-Brentano geometry. Intensity data were recorded using an X'Celerator detector and 2θ scans in the range of 5-40° were performed. During the experiment the powdered sample was exposed to Cu-Kα radiation (λ = 1.5418 Å). The PXRD patterns of the as-synthesised (**COB1-DMF)** and activated **(COB-act)** samples were recorded at 298 K.

Single-crystal X-ray Diffraction

Single crystal X-ray diffraction data were collected on a Bruker APEX-II Quasar CCD area-detector diffractometer equipped with an Oxford Cryostream 700Plus cryostat, and on a Bruker D8 Venture diffractometer equipped with a PHOTON II CPAD detector and an Oxford Cryostream 800Plus cryostat. A multilayer monochromator with $Mo_{K\alpha}$ radiation (λ = 0.71073 Å) from an Incoatec $I_{\mu S}$ microsource was used. Data reduction was carried out by means of standard procedures using the Bruker software package SAINT[2] and absorption corrections and the correction of other systematic errors were performed using SADABS.[3] The structures were solved by direct methods using SHELXS-2016 and refined using SHELXL-2016[4] and X-Seed[5] or Olex2[5] were used as the graphical interface for the SHELX program suite. Hydrogen atoms were placed in calculated positions using riding models.

Environmental gas cell experiments

An environmental gas cell (developed in-house) was used to determine the crystal structures of the various phases at 298 K under controlled pressures by means of single-crystal X-ray diffraction. First, the structure of **COB1^{0}** was determined under vacuum after activating a crystal of **COB1-DMF**. The structure of **COB1-CO2^{10}** was determined after pressurising **COB1^{0}** with 10 bar of CO_2 gas for 8 hours. The structure of **COB1-CO2^{19}** was determined after pressurising the crystal of **COB1-CO2^{10}** with 19 bar CO_2 and allowing it to equilibrate for 8 hours. The structure of **COB1-CO2^{30}** was determined after pressurising **COB1-CO2^{19}** with 30 bar CO_2 and equilibrating for 8 hours. We note that $R1$ for the gas-loaded structures increases with pressure, and this is most likely due to increasing strain experienced by the crystal.

Volumetric Sorption Analysis

A Setaram PCTPro-E&E gas sorption analyser with a MicroDoser attachment was utilised to conduct high pressure gas sorption experiments with CO_2 and N_2. The instrument utilises Sievert's volumetric method. The sample temperature was maintained to an accuracy of ±1 °C using a Grant refrigerated recirculation bath filled with antifreeze and water. A sample at known pressure and volume was connected to a reservoir of known volume and pressure through an isolation valve. The valve was opened, and the system allowed to equilibrate. The difference between the measured and calculated pressures was used to determine the amount of gas adsorbed. National Institute of Standards and Technology (NIST) software was used to calculate the thermodynamic corrections to account for the non-ideal behaviour of the gases at relatively high pressures. The PCTPro-E&E with the MicroDoser attachment is used for small sample sizes and has a range of vacuum to 60 bar. Sample sizes of 80 mg were used and activated in situ using vacuum and heat, if necessary. Blank runs for each gas were recorded to further correct for any other residual systematic errors in the experiment. Figure preparation and data analyses were performed using Microsoft Excel and OriginPro.

Pressure-Gradient Differential Scanning Calorimetry for CO_2 (PG-DSC)

Experiments were carried out using a Setaram Micro-DSC7 Evo instrument. Heat flow was recorded at 298 K in the pressure range of 4-35 bar for CO_2 at 298 K.

Table S1. Crystallographic table of **COB1** under controlled pressure of CO_2.

Complex	**COB1-DMF**	**COB1^{0}**	**COB1-CO2^{10}**	**COB1-CO2^{19}**	**COB1-CO2^{30}**
Temperature (K)	100	298	298	298	298
Empirical formula	$C_{51.50}H_{53.50}Co_2N_{6.50}O_{12.50}$	$C_{44}H_{36}N_4O_{10}Co_2$	$C_{44.9}H_{36}N_4O_{11.8}Co_2$	$C_{45}H_{36}N_4O_{13}Co_2$	$C_{47}H_{36}N_4O_{16}Co_2$
Formula weight	1081.36	898.66	938.23	958.64	1030.66
Wavelength (Å)	0.71073	0.71073	0.71073	0.71073	0.71073
Crystal system	monoclinic	monoclinic	monoclinic	monoclinic	monoclinic
Space group	$P2_1/n$	$C2/c$	$C2/c$	$C2/c$	$C2/c$
a, (Å)	29.7813(12)	23.7504(14)	23.7632(11)	30.071(3)	30.075(5)
b, (Å)	15.7987(7)	9.7971(6)	9.8043(5)	7.8976(6)	7.8801(13)
c, (Å)	23.7492(9)	20.3230(12)	20.3897(10)	23.8471(17)	23.860(4)
β, (°)	101.808(2)	104.156(2)	102.360(2)	101.951(4)	102.013(4)
Volume (Å^3)	10937.7(8)	4585.3(5)	4640.3(4)	5540.6(8)	5531.0(16)
Z	8	4	4	4	4
Calculated density (g cm^{-3})	1.313	1.302	1.343	1.149	1.238
Absorption coefficient (mm^{-1})	0.671	0.781	0.772	0.646	0.647
F_{000}	4496	1848	1927	1968	2112
Approx. Crystal size (mm^3)	0.300 × 0.170 × 0.100	0.268 × 0.135 × 0.088	0.268 × 0.135 × 0.088	0.268 × 0.135 × 0.088	0.268 × 0.135 × 0.088
θ range for data collection (°)	1.97 to 26.0	2.26 to 26.45	2.21 to 25.09	1.99 to 26.8	1.99 to 21.3
Miller index ranges	-36 ≤ h ≤ 36 -19 ≤ k ≤19 -36 ≤ l ≤ 36	-29 ≤ h ≤ 29 -12 ≤ k ≤ 12, -25 ≤ l ≤ 2	-28 ≤ h ≤ 28 -11 ≤ k ≤11 -24 ≤ l ≤ 24	-37 ≤ h ≤ 36, 0 ≤ k ≤ 9 0 ≤ l ≤ 30	-35 ≤ h ≤ 35 -9 ≤ k ≤ 9 -28 ≤ l ≤ 28
Reflections collected	135400	60406	55175	11597	144436
Independent reflections	21507 R_{int} = 0.1097 R_{sigma} = 0.0818	4721 R_{int} =0.1258 R_{sigma} = 0.0611	4116 R_{int} = 0.1010 R_{sigma} = 0.0448	5776 R_{int} = 0.1658 R_{sigma} =0.1368	4952 R_{int} = 0.2636 R_{sigma} =0.0658
Completeness to θ max (%)	0.995	99.9	99.5	98.0	99.9
Refinement method	Full-matrix least-squares on F^2				
Data / restraints / parameters	21507 / 0 / 1081	4721 /0 / 271	4116 / 0 / 271	5776 / 48 / 430	4952 / 0 / 462
Goodness-of-fit on F	1.021	1.034	1.021	1.236	1.120
Final R indices [I > 2 Θ(I)]	$R1$ = 0.0848 $wR2$ = 0.2354	$R1$ = 0.0494 $wR2$ = 0.1000	$R1$ =0.0428 $wR2$ = 0.0843	R1 = 0.1368 $wR2$ = 0.2858	$R1$ = 0.1143 $wR2$ = 0.2554
R indices	$R1$ = 0.1453 $wR2$ = 0.2855	$R1$ = 0.1217 wR_2 = 0.1371	$R1$ = 0.0791 wR_2 = 0.0983	$R1$ = 0.1658 $wR2$ = 0.3045	$R1$ = 0.1594 $wR2$ = 0.2956

Table S2. Structural phase classification at 298 K.

COB1-DMF	As-synthesised version containing DMF guest molecules
COB1^{0}	Host framework determined under vacuum
COB1-CO2^{10}	Form determined under 10 bar of CO_2 gas pressure
COB1-CO2^{19}	Form determined under 19 bar of CO_2 gas pressure

COB1-CO2^{30}	Form determined under 30 bar of CO_2 gas pressure

Table S3. Selected distances and angles of **COB1-DMF** and **COB1^{x}** under controlled CO_2 pressures.

Compound	OBA length ($centroid_{SBU}\cdots centroid_{SBU}$) (Å)	OBA Bend angle ($centroid_{SBU}\cdots O_{ether}\cdots centroid_{SBU}$) (°)	BPMP length ($centroid_{SBU}\cdots centroid_{SBU}$) (Å)	Acute angle of pyrazine relative to P_{ac} (°)	Co···Co distance (Å)	Paddlewheel acute angle with P_{ac} (°)
COB1-DMF	14.263	119.764	19.029	26.401	2.629	43.910
COB1^{0}	14.141	119.208	18.902	84.11	2.749	35.892
COB1-CO2^{10}	14.144	119.288	18.906	83.903	2.749	35.885
COB1-CO2^{19}	14.302	120.444	19.142	25.662	2.727	43.991

1. TGA thermograms

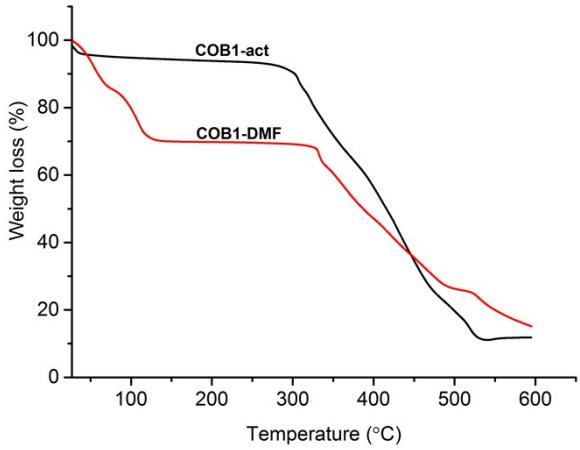

Figure S1. TGA of **COB1-DMF** and **COB1-act**.

2. Unit cell dimensions and volume as a function of pressure

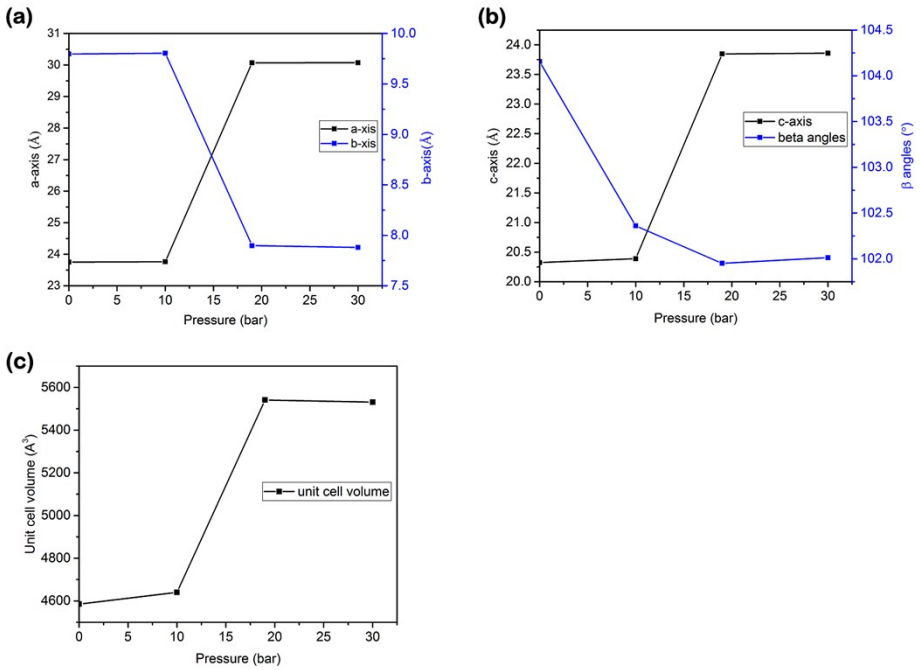

Figure S2. Changes in unit cell parameters for the VP-SCD structures **COB1^{x}**, where x = 0, 10, 19 and 30. In situ data were collected at 298 K.

3. Variable temperature PG-DSC under CO_2 pressure

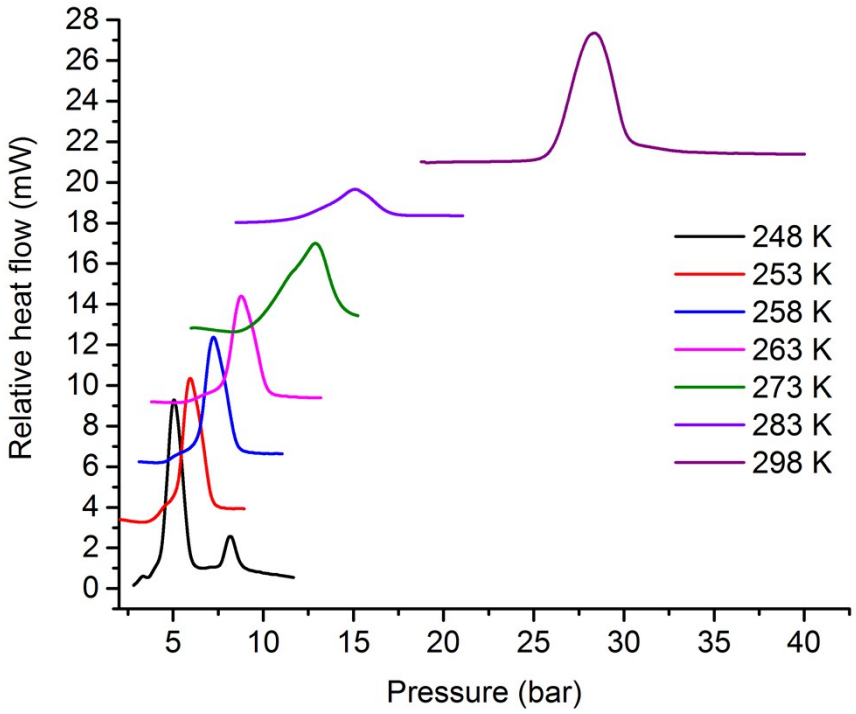

Figure S3. Variable temperature PG-DSC under CO_2 gas pressure.

4. Theoretical investigation

Owing to positional disorder, the apohost crystallographic models obtained under CO_2 pressure were geometry optimized using the CASTEP[6] code implemented in Materials Studio.[7] The density functional theory (DFT) generalised gradient approximation of Perdew-Burke-Ernzerhof (PBE)[8] in combination with Grimme's DFT-D dispersion correction[9] was employed with on the fly generated Vanderbilt-type ultrasoft pseudopotentials[10] in combination with the Koelling-Harmon scalar-relativistic approach[11] and a planewave expansion to an energy cutoff of 489.8 eV. Integration in the reciprocal lattice was performed using a Monkhorst-Pack grid[12] with a 0.05 $Å^{-1}$ k-point separation and self-consistent field convergence was set to 2.0×10^{-6} eV. A 50% admixture of the charge density[13] was applied in conjunction with a DIIS (direct inversion in an iterative subspace) [14] size of 20 to speed up convergence. Convergence tolerances for geometry optimization using the BFGS (Broyden-Fletcher-Goldfarb-Shanno) algorithm[15] were set to 2.0×10^{-5} eV $atom^{-1}$, 0.05 eV $Å^{-1}$ and 0.002 Å on energy, maximum force and maximum displacement respectively. To reduce computational expense, calculations were carried out in the primitive cell representation with

$$a' = b' = \sqrt{a^2 + b^2}/2$$

$$c` = c$$

$$\cos(\gamma'/2) = a/\sqrt{a^2 + b^2}$$

$$\cos^2\alpha' = \cos^2\beta' = \frac{\sin^2\gamma' - \left(2ab\sin\beta/(a^2 + b^2)\right)^2}{2 - 2\cos\gamma'}$$

since $V' = V/2$, as shown in Figure S4.

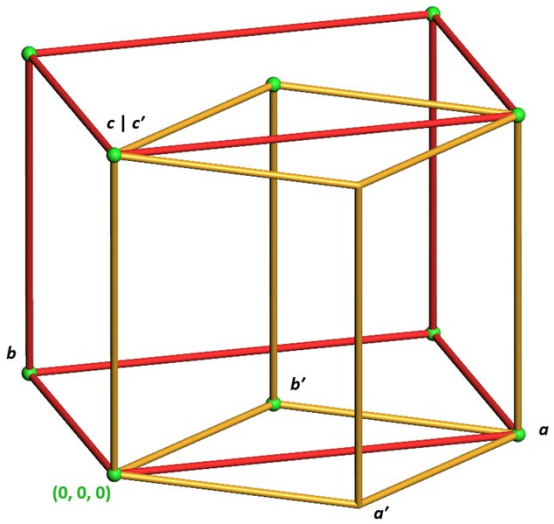

Figure S4. Overlay of conventional and primitive representations of a face-centred monoclinic unit cell in red and orange, respectively. Lattice points are indicated as green spheres.

Table S3. Guest-omitted unit cell energies (kcal mol^{-1}) relative to that of **COB1[0]**.

COB1-DMF	54.65
COB1[0]	0
COB1-CO2[10]	0.058
COB1-CO2[19]	45.26
COB1-CO2[30]	56.36

Attempting to model the CO_2-induced gate opening through an incremental perturbing of the unit cell parameters (10 bar → 19 bar) rendered the ligands far removed from their crystallographic orientations. A linear synchronous transit approach was subsequently applied to geometrically follow the structural transformation.[16] A molecular fragment representing a complete coordination sphere of the Co_2OBA_2 paddlewheel was extracted from the geometry optimised 10 bar and 19 bar crystal structures and each atom paired after translocation to the same origin. The resulting pathway shown in Video S1 reveals a major contortion of the BPMP ligand, while the Co_2OBA_2 paddlewheel undergoes a reorientation. Since OBA links paddlewheels along the (0±12) Miller planes, viewing down [0±21] sheds light on the BPMP contribution to the transformation. Similarly, BPMP bridges paddlewheels along (3±10) allowing the [1±30] view to highlight the contortion of the OBA ligand. The rotation of the piperazine moiety from nearly perpendicular (83.90°) to acute (25.66°) during the course of the transformation is discernible in the view down the *c* axis in **Figure S4** below.

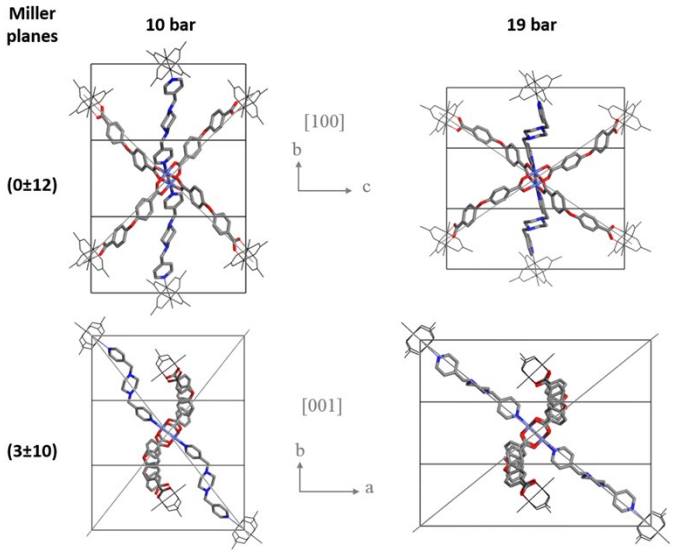

Figure S4. Comparison of CO_2-adsorption induced gate opening structural transformation. Miller planes along which the two ligands interconnect paddlewheel moieties are shown.

5. Description of video files

Video S1 shows the CO_2-induced gate opening transformation of the framework from **COB1-CO2^{10}** to **COB1-CO2^{19}**. Expanding the mechanism derived for the fragment into a crystallographic representation, Video S2 shows the gradual increase in solvent-accessible space. These video files are best viewed with the video player set to loop.

References

1. D. Pocic, J. Planeix, N. Kyritsakas, A. Jouaiti, M. Hosseini, *CrystEngComm*. 2005, **7**, 624.
2. *SAINT Data Reduction Software*, Version 6.45; Bruker AXS Inc., Madison, WI, 2003.
3. (a) *SADABS*, Version 2.05; Bruker AXS Inc., Madison, WI, 2002; (b) Blessing, R. H. *Acta Crystallogr., Sect. A: Found. Crystallogr.* 1995, **51**, 33.
4. G. M. Sheldrick, *Acta Crystallogr., Sect. A: Found. Crystallogr.* 2008, **64**, 112.
5. (a) L. J. Barbour, *J. Supramol. Chem.* 2001, **1**, 189; (b) L.J. Bourhis, O.V. Dolomanov, R.J. Gildea, J.A.K. Howard, H. Puschmann, *Acta Cryst*. 2015. **A71**, 59.
6. S. J. Clark, M. D. Segall, C. J. Pickard, P. J. Hasnip, M. J. Probert, K. Refson, M. C. Payne, Z. *Kristallogr*. *2005*, **220**, 567.
7. Dassault Systèmes BIOVIA, Materials Studio, Release 18, San Diego: *Dassault Systèmes,* 2017.
8. J. P. Perdew, K. Burke, M. Ernzerhof, *Phys. Rev. Lett*. 1996, **77**, 3865
9. S. Grimme, J. *Comput. Chem.* 2006, **27**, 1787.
10. D. Vanderbilt, P*hys. Rev*. *B* 1990, **41**, 7892.
11. D. D. Koelling, B. N. Harmon, *J. Phys. C* 1977, **10**, 3107.
12. H. J. Monkhorst, J. D. Pack, P*hys. Rev. B* 1976, **13**, 5188.
13. G. Kresse, J. Furthmuller, *Phys. Rev. B* 1996, **54**, 11169.
14. P. Pulay, C*hem. Phys. Lett*. 1980, **73**, 393.
15. B. G. Pfrommer, M. Cote, S. G. Louie, M. L. Cohen, *J. Comput. Phys*. 1997, **131**, 233.
16. A. Halgren, W. N. Lipscomb, *Chem. Phys*. Lett. 1977, **49**, 225.